Why Did Ozone Concentrations Remain High During Shanghai's Static Management? A Statistical and Radical Chemistry Perspective

Jian Zhu[1], Shanshan Wang[1,2], Chuanqi Gu[1], Zhiwen Jiang[1], Sanbao Zhang[1], Ruibin Xue[1], Yuhao Yan[1], Bin Zhou[1,2,3]

[1]Shanghai Key Laboratory of Atmospheric Particle Pollution and Prevention (LAP³), Department of Environmental Science and Engineering, Fudan University, Shanghai, 200433, China.

[2]Institute of Eco-Chongming (IEC), Shanghai, 202162, China.

[3]Institute of Atmospheric Sciences, Fudan University, Shanghai, 200433, China.

Correspondence to: Bin Zhou (binzhou@fudan.edu.cn) and Shanshan Wang (shanshanwang@fudan.edu.cn)

Abstract

During the period of April and May 2022, Shanghai implemented city-wide static management measures to control the spread of the Omicron variant. Compared to the lockdown in early 2020, the static management in 2022 occurred during the high-ozone season and lasted for a longer duration. It can be considered as a "large-scale field experiment" to study the response of ambient ozone levels to emission reductions. During this period, we conducted comprehensive observations at Fudan University Jiangwan Campus in the northeast corner of Shanghai. Similar experiments were also conducted during the same period in 2020 and 2021. Despite the significant reduction of approximately 30% in VOCs and around 50% in NO_2 due to static management in 2022, the average ozone level increased by nearly 23%, compared to 2020 and 2021. This suggests that the reduction in ozone precursors and other pollutants did not lead to a corresponding decrease in ozone concentrations as expected. Cluster analysis of diurnal patterns of ozone concentration revealed four distinct types of diurnal ozone variations. Cluster 3 and Cluster 4, with high ozone levels, experienced significant increases in their share during static management, ultimately leading to an overall increase in average ozone levels in 2022. According to the Observation-Based Model (OBM) simulation analysis, the average peak concentrations of OH, HO_2, and RO_2 in 2022 were estimated to be 5.1×10^6, 4.7×10^8, and 2.6×10^8 molecules cm^{-3}, respectively, representing an increase of about 30% compared to the levels in 2020 and 2021. Although HONO photolysis was the main contributor to the primary source of ROx radicals, the radical cycling process remained dominant for the overall production of ROx radicals. Due to a significant decrease in NO_2 concentration relative to VOCs, the average $VOCs/NO_2$ ratio increased from 1.6 in 2020 to 3.0 in 2022, which is also reflected in the radical cycling. The ratio of OH radical propagation (OH+VOCs) to termination (OH+NO_2) was 2.37, higher than 1.18 in 2020 and 1.78 in 2021, indicating that the different reduction proportions of precursors led to a higher $VOCs/NO_2$ ratio, strengthening the radical cycling. The differential reduction in precursor VOCs and NO_2 levels due to static management is the underlying cause for the increase in ozone concentration in Shanghai.

1 Introduction

To curb the spread of Omicron variant in Shanghai, China, the local government decided to implement city-wide static management in early April 2022. The strict two-month lockdown severely impacted the economic activities and human life of this mega city. According to official statistics (https://tjj.sh.gov.cn/sjfb/index.html), in April and May 2022, Shanghai experienced a year-on-year decrease of 42% in its total industrial output value. Moreover, the total volume of transported goods decreased by 30% year-on-year, with road transport witnessing a significant drop of 64%. Additionally, the port cargo

throughput decreased by 31% year-on-year. The direct effect of such lockdown policies on air quality is a significant reduction in anthropogenic emissions, which can be considered as an ideal experiment on emissions control in a mega-city to explore the reduction potential and response of air quality . It makes sense to take advantage of this rare yet regrettable window to study the causes and management of air pollution, especially in countries like China that face complex air pollution issues.

Prior to this, China had implemented a series of nationwide lockdown measures against the occurrence and spread of the virus in early 2020. This reduction in human activity is expected to significantly reduce air pollutant emissions, as confirmed by lots of studies on lockdown in 2020 (Bao and Zhang, 2020; Huang et al., 2021; Li et al., 2021b; Liu et al., 2020; Tian et al., 2021; Wang et al., 2021; Zhang et al., 2022b). Reports on the impact of the lockdown on air quality most commonly focus on measuring nitrogen dioxide (NO_2) and fine particulate matter ($PM_{2.5}$) (Agarwal et al., 2020; Hua et al., 2021; Chu et al., 2021). According to satellite data, tropospheric nitrogen oxides (NO_x) emissions have decreased by 30-60% compared to pre-lockdown levels (Feng et al., 2020; Ding et al., 2020; Venter et al., 2020). Similarly, surface $PM_{2.5}$ levels in northern China have also decreased by approximately 35%. Meanwhile, the average O_3 concentration has increased 1.5-2 times (Shi and Brasseur, 2020). In Wuhan, the urban area that implemented stringent measures to limit the spread of the coronavirus, concentrations of $PM_{2.5}$, NO_2, and ozone also exhibited similar changes (Shi and Brasseur, 2020). Among these pollutants, NO_2 from traffic sources has shown the most significant reduction, with traffic-related NO_2 exhibiting the largest decrease (Rana et al., 2021; Wang et al., 2020). Huang et al. (2021) suggest that increase in O_3 enhances atmospheric oxidation capacity, providing favorable conditions for the formation of secondary particulate matter. Due to the lockdown taking place during winter, which is a season of high particulate matter pollution in China, the reports on the impact of the lockdown on air quality have focused more on the changes in particulate matter. The lockdown in Shanghai in 2022 was implemented in April and May during the high-ozone (O_3) season and lasted for a longer duration, providing an opportunity to study atmospheric pollution primarily caused by O_3.

Previous extensive research has demonstrated that the formation of O_3 in response to its precursors is highly nonlinear, rather than linear, which presents a challenge in ozone control (Liu and Shi, 2021; Wang et al., 2017; Sillman, 1999). The COVID-19 pandemic provided a costly experiment to validate this. During the static management period in Shanghai, despite a reduction in precursor emissions, the ozone levels increased compared to the previous year. The cause of this increase is attributed to an imbalance in the reduction ratio of nitrogen oxides (NO_x) and volatile organic compounds (VOCs) rather than meteorological conditions, according to satellite observation results (Tan and Wang, 2022; Xue et al., 2022). In this current study, aim is to elucidate the reasons behind the increase in ozone levels in Shanghai through a comprehensive approach involving in-situ observations, mathematical analysis, and modeling. Benefitting from our conducted routine observational campaigns, we have obtained comprehensive observational data for both the static management period and corresponding historical periods. We initiated our analysis by comparing pollutant levels and diurnal variations during the static management period with those from historical reference periods. Subsequently, by clustering diurnal ozone profile patterns, we examined the reasons behind the elevated ozone levels from a statistical perspective. Furthermore, we discuss changes in radical chemistry compared to historical periods, shedding light on the increase in ozone concentrations from a photochemical process standpoint. It is worth mentioning that, based on previous researchs and our analysis, meteorological conditions are not considered to be the primary cause of the ozone increase during the static management period, even though we acknowledge that meteorological conditions are indeed important factors influencing ozone levels. The in-depth comparison of meteorological conditions is presented in Text S1 of the Supplement.

2 Experimental Details and Methods

2.1 Location and Experimental Setup

During the static management period in April and May of 2022, we conducted comprehensive observational experiments at Fudan University's Jiangwan Campus (31.34°N, 121.51°E), located in an urban area in northeastern Shanghai, China. Similar experiments were also conducted during the corresponding period in 2020 and 2021. The ambient concentrations of O_3, NO_2, SO_2, HONO, and HCHO were measured using the Differential Optical Absorption Spectroscopy (DOAS) system located on the rooftop of the Environmental Science Building (Zhu et al., 2020; Guo et al., 2021; Zhu et al., 2022). Based on the given optical path length and integration time, the detection limits for O_3, NO_2, SO_2, HONO, and HCHO were approximately 1.3 ppbv, 0.5 ppbv, 0.1 ppbv, 0.1 ppbv, and 0.5 ppbv, respectively. The measurements were carried out with a time resolution of 5-6 minutes and detailed fitting configurations are available in Table S1. Non-methane volatile organic compounds (NMVOCs) were monitored in real-time using the TH-300B online monitoring instrument, which has been previously described in detail in previous reports (Gu et al., 2022; Zhu et al., 2020). The photolysis rate of NO_2 ($j(NO_2)$) was measured using a filter radiometer (Meteorologieconsult Gmbh, Germany). The meteorological parameters data such as pressure (P), temperature (TEMP), relative humidity (RH), wind speed (WS), wind direction (WD), and boundary layer height (BLH) are derived from the European Center for Medium-Range Weather Forecasts (ECMWF) atmospheric reanalysis product ERA5 and extracted from the nest where the measurement site is located. The PM$_{2.5}$ data was obtained from the Yangpu environment monitoring station (31.53°N, 121.25°E) near the measurement site.

2.2 Observation-Based Model (OBM)

The open-source zero-dimensional box model tool AtChem2 was used to simulate atmospheric chemical processes, which is specifically designed for use with the Master Chemical Mechanism (MCM) (Sommariva et al., 2020). The MCM, one of most widely used chemical mechanism for chemistry, is a near-explicit chemical mechanism which describes the degradation of methane and 142 nonmethane VOCs and over 17000 elementary reactions of 6700 primary, secondary and radical species (http://mcm.york.ac.uk/, last access: 16 January 2023) (Jenkin et al., 2003; Saunders et al., 2003). AtChem2 software and documentation can be found on https://github.com/AtChem/ (last accessed on January 16, 2023).

In this study, the observed data of O_3, NO_2, SO_2, HONO, HCHO, NMVOCs, $j(NO_2)$, P, T, RH, and BLH were used as inputs to constrain the model calculations. The photolysis rates of other molecules such as O_3, HCHO, HONO, and OVOCs can be calculated in this model platform with the basic principle driven by the solar zenith angle and scaled by the measured J_{NO2} (Sommariva et al., 2020). The removal of all unconstrained and simulated species caused by the deposition is determined by a parameterization approach, and is determined by the accumulation of the deposition velocity of 0.01 m s^{-1} within the boundary layer (Santiago et al., 2017). The sensitivity of simulation results to the deposition velocity has been studied in previous research, and the impact is limited (Zhu et al., 2020). The model outputs include the concentration of the hydroxyl radical (OH) and hydroperoxy radical (HO$_2$), as well as the reaction rates at each step of the simulation process.

2.3 Machine learning

Two machine learning methods, k-means clustering and the stacking model, were utilized in this study. In order to investigate the reasons for the overall increase in ozone levels during the static management period from the perspective of its diurnal variation, the k-means clustering method was applied to cluster 24-hour time series of O_3 concentration (Zhang et al., 2004). Time-series clustering is a specific application of curve clustering, which is similar to trajectory clustering in the transport of air masses

(Darby, 2005; Suris et al., 2022). The procedure for k-means clustering is as follows: (i) randomly initialize k clusters and then calculate the cluster centroid or mean, (ii) assign each data point to the nearest cluster using an appropriate distance measure, (iii) re-calculate the cluster centroids based on the current cluster members, (iv) repeat steps ii and iii until there is no further change. Additionally, the stacking model was applied to address missing values in DOAS observations caused by uncontrollable factors, ensuring the continuity and variation characteristics of the data. This step was deemed necessary for two main reasons. Firstly, the clustering analysis of O_3 diurnal variation demands a continuous time series without any missing values. Secondly, compared to the conventional method of handling missing data in the input of the OBM model through simple linear interpolation, the stacking model preserves the diurnal variation characteristics of the data, ensuring the correct constraints on the OBM model. The stacked model is an ensemble machine learning algorithm that consists of two levels, with two or more base models at level 0 and one meta-model at level 1. The meta-model is trained using predictions made by the base models on out-of-sample data. In other words, data that was not used to train the base models is fed into them to make predictions. These predictions, along with the corresponding expected outputs, form the input and output pairs of the training dataset used to fit the meta-model. The stacking model has been previously described in detail and demonstrated good performance in Zhu et al. (2022), and the architecture of the stacking model can also be found in Figure S1. In this study, the models for O_3, NO_2, SO_2, HONO, and HCHO demonstrated good performance, as shown in Figure S2-S6 of the Supplement.

3 Results and Discussion

3.1 Year-on-year changes on air quality

Figure 1 compares the average levels of the meteorological parameters and air pollutants during the period from April to May of 2020 to 2022, while Figure 2 compares the diurnal variations. In terms of meteorological parameters, the temperature and relative humidity, and $j(NO_2)$ during the static management period in 2022 were almost unchanged compared to the same period in 2020 and 2021. The average temperature difference in 2022 was 6.5°C, which was similar to that of 2020 and slightly higher than that of 2021, while the average relative humidity at noon in 2022 was also comparable to that of 2020 and was 5% lower than that of 2021. Furthermore, we also ruled out the contribution of transport from the surrounding areas to the increase in ozone concentration in Shanghai during the 2022 static management period (see Figures S7-S10).The abrupt reduction of emissions across the entire industry led to a significant decrease in primary pollutant concentrations. The average concentrations of $PM_{2.5}$ in April and May from 2020 to 2022 were 36.8 ± 24.1, 30.0 ± 23.1, and 21.8 ± 14.0 ug m^{-3}, respectively, showing a decreasing trend over the years. And the diurnal variation profile in Figure 2d shows that $PM_{2.5}$ levels decreased proportionally throughout the entire 24-hour period, without any particularly prominent periods of decrease. The VOCs and NO_2 declined by 29% and 55% respectively compared to 2020, and by 35% and 51% respectively compared to 2021. Due to the significant decrease in NO_2 concentration compared to VOCs, the average ratio of VOCs/NO_2 has increased from 1.6 in 2020 to 3.0 in 2022. However, the precursor reduction at different magnitudes has led to an increase of approximately 23% in the average level of ozone. The photochemical production of ozone is controlled by the non-linear chemistry of the precursors VOCs and NOx (NO_2+NO). The literatures have shown that Shanghai in the spring largely operates under VOCs-limited regime (Li et al., 2021a; Xue et al., 2022). Therefore, the reduction in VOCs during the static management period may not be enough to counteract the titration effect of NOx, and may even alter the ozone formation regime in Shanghai. From the perspective of diurnal variation (see Figure 2), the period with a significant difference in the magnitude of the decrease between VOCs and NO_2 occurred during the strong photochemical process in the morning until noon. Therefore, the VOCs/NO_2 ratio during the static management period was significantly higher in the morning compared to the same period in 2020 and 2021. The weakening of the titration of nitrogen

oxides on ozone during nighttime led to significantly higher nighttime average levels during the static management period compared to 2020 and 2021. Due to the higher O_3 baseline concentration and higher $VOCs/NO_2$ ratio, there was a significant increase in overall ozone levels.
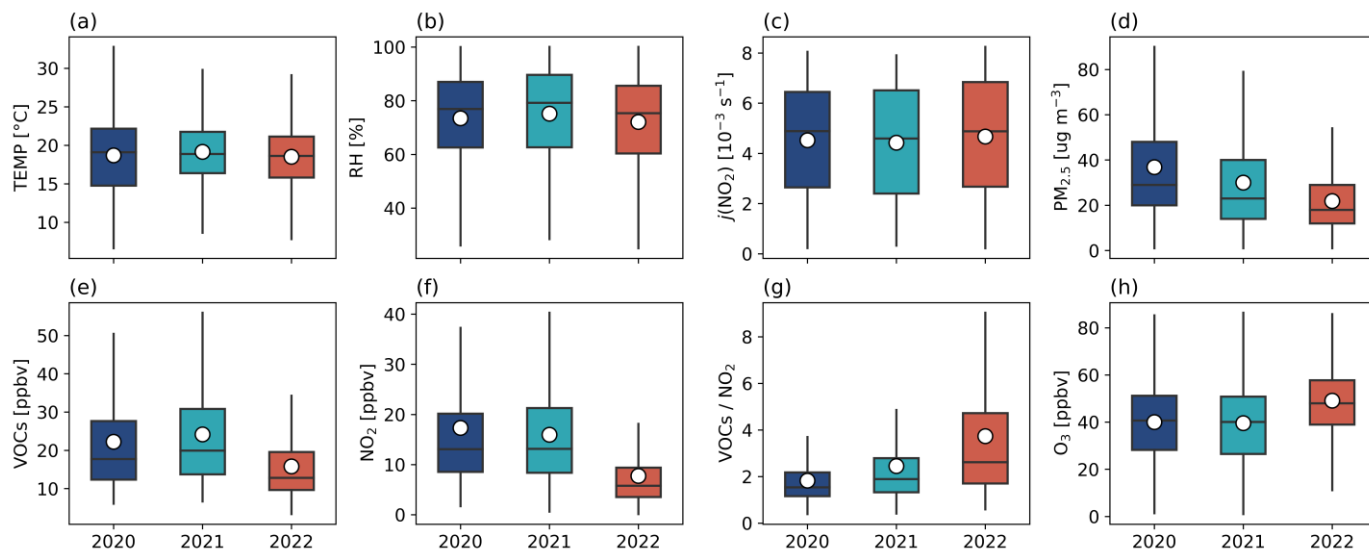
Figure 1. Comparison of meteorological parameters (TEMP, RH, $j(NO_2)$) and air pollutants ($PM_{2.5}$, VOCs, NO_2, $VOCs/NO_2$, O_3) during the periods from April to May of 2020, 2021, and 2022. The top and bottom of the vertical line for each box correspond to the 95th and 5th percentiles, respectively. The dots represent the averages, and the top, middle, and bottom lines of the box mark the 75th, 50th, and 25th percentiles, respectively.
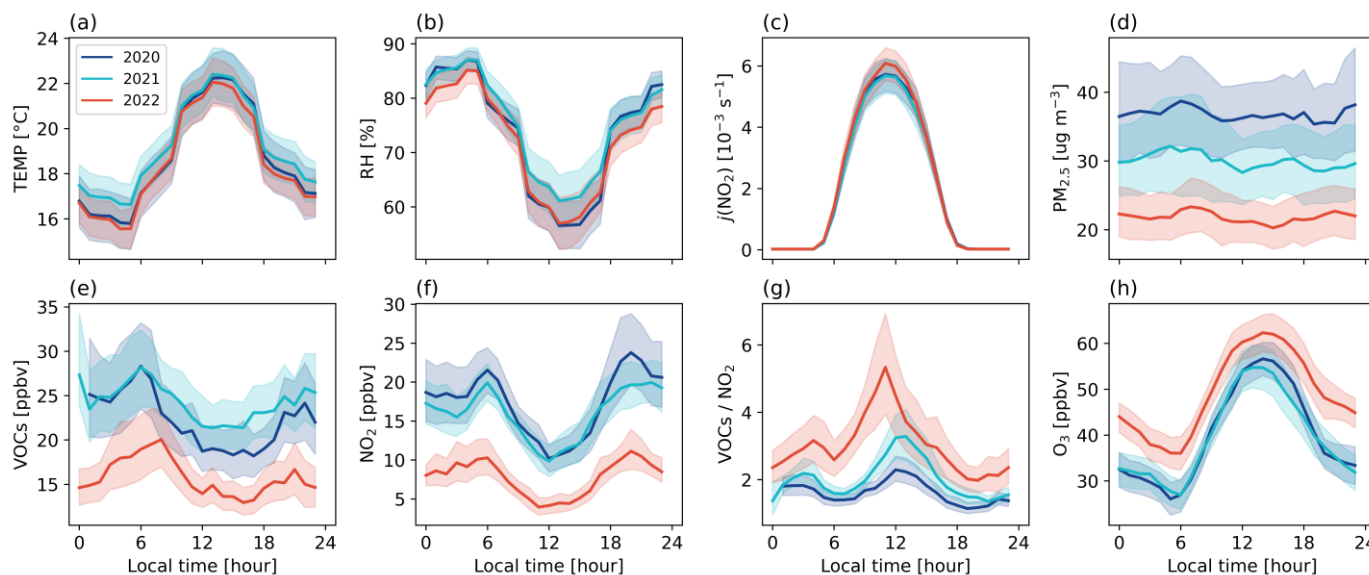
Figure 2. The mean diurnal profiles of meteorological parameters and air pollutants during the periods from April to May of 2020, 2021, and 2022. Colored areas denote 95% confidence intervals.

As VOCs are crucial precursors for ozone formation, we conducted a comparison of each VOCs component during the 2022 static management period with those of the same period in 2020 and 2021, as shown in Figure 3. We classified the 103 VOCs into six categories based on functional groups, including alkanes, alkenes, alkynes, aromatics, oxygenated VOCs (OVOCs), and halohydrocarbons. The detailed classification is available in the Table S2. The results revealed that aromatics experienced the most significant year-over-year reduction in absolute terms. The chemical raw materials and chemical products manufacturing industry, which is the main source of aromatics (Liu et al., 2019), accounts for 10% of the total industrial output value, and this industry experienced a 32% year-on-year decrease in total output value during the static management period

(https://tjj.sh.gov.cn/sjfb/index.html). In contrast, OVOCs remained relatively stable, primarily because they are sourced from biogenic (Liu et al., 2019), and thus, were less impacted by lockdown measures relative to other VOCs. From the perspective of ozone formation potential (OFP), in the years 2020 and 2021, the primary contributors were aromatics, followed by alkenes, while in 2022, the primary contributors shifted to alkenes, with OVOCs coming in second (see Text S4 and Figure S11).

The reduction in the imbalance of VOCs has altered the average proportion of each component. Specifically, the proportion of aromatics decreased from 8.9% and 11.5% to 4.1%, while the proportion of OVOCs increased from 12.7% and 13.7% to 17.2%. The photolysis of OVOCs is a major source of the important radicals ROx (OH+HO$_2$+RO$_2$) in the photochemical cycle, with a daily average contribution rate of over 30% (Xue et al., 2016). In the radical chemistry section, the photolysis of OVOCs, as well as the reactions of O$_3$ and NO$_3$ with VOCs, have been quantified for their contributions to the radicals. Additionally, the role of VOCs in the propagation of radicals has been quantified.. The mean diurnal profiles of the VOCs indicated that the daily average concentration range in 2020, 2021, and 2022 was between 18-28 ppbv, 21-28 ppbv, and 13-20 ppbv, respectively.

In 2022, the peak time of VOCs was observed at 08:00, which exhibited a delay compared to the peak times observed in 2020 and 2021 at 06:00, resembling the previously reported "weekend effect" on VOCs that the peak time of VOCs is delayed on weekends in comparison to weekdays (Cai et al., 2010). In Figure S12 of Supplement, we observe that the peak of VOCs diurnal profile in June 2023, after the lifting of restrictions, returned to 06:00. This finding indicates that the reduced human activities during the 2022 period, similar to weekends, led to a decline in anthropogenic VOC emissions in the morning.
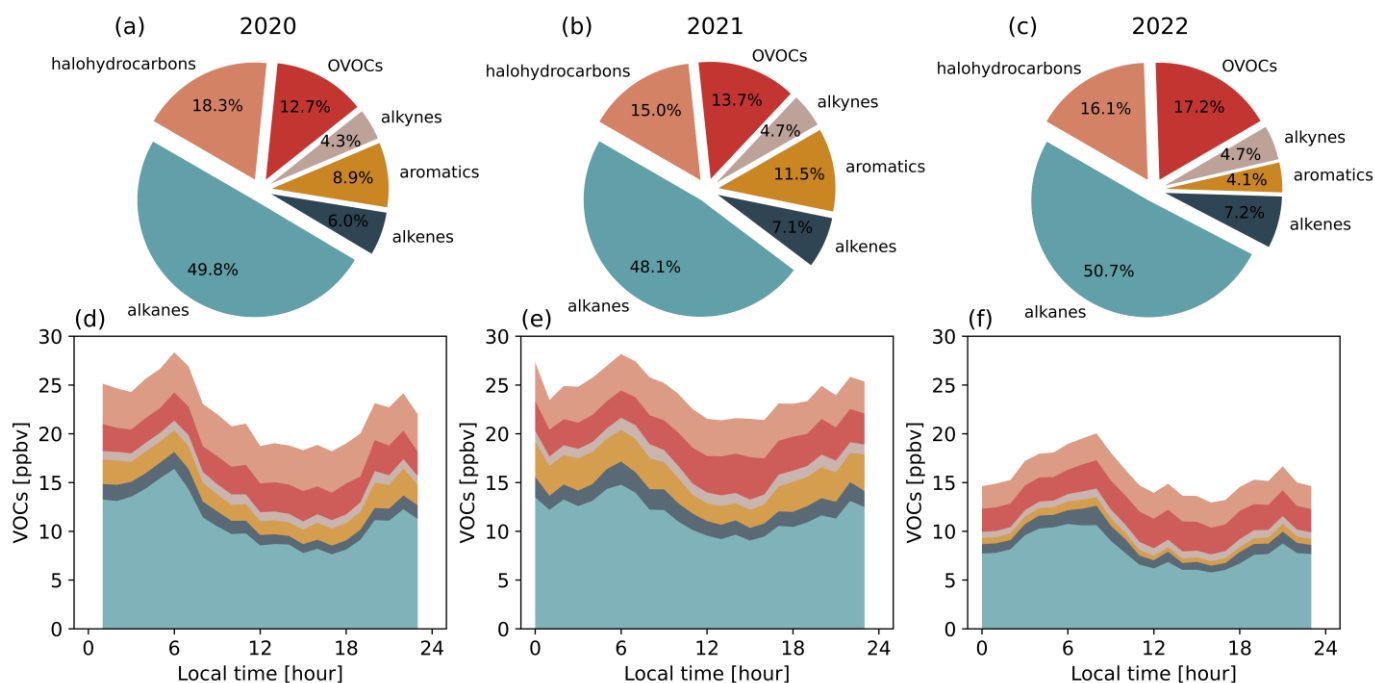
Figure 3. The proportions (a, b, c) and the mean diurnal profiles (d, e, f) of different VOCs components during the periods from April to May of 2020, 2021, and 2022.

3.2 Clustering of O$_3$ diurnal profiles

The k-means algorithm clustered the ozone diurnal profiles over the three years into four types, as shown in Figure 4a. We define the minimum concentration in the ozone diurnal profile as the background concentration, and the difference between the midday peak and the morning trough represents the net ozone production. These four types of profiles can be described as follows: Cluster 1 with low background concentration (22.4 ppbv) and low net production (14.8 ppbv); Cluster 2 with low background

192 concentration (16.9 ppbv) and high net production (45.9 ppbv); Cluster 3 with high background concentration (40.6 ppbv) and

193 low net production (17.5 ppbv); and Cluster 4 with high background concentration (33.3 ppbv) and high net production (50.9

194 ppbv). The background concentration of ozone is mainly determined by the nighttime loss of ozone and the titration of nitrogen

195 oxides in the morning, while the net production depends on the intensity of the photochemical reactions. In Figure 4b, the four

196 ozone profiles occurred for 13, 24, 20, and 4 days in 2020, comparable occupation of 19, 21, 17, and 4 days in 2021, respectively.

197 During the static management period of 2022, when the nitrogen oxide titration effect weakened, the number of days on which

198 Cluster 3 and Cluster 4 appeared increased to 34 and 16, respectively. The average ozone levels for the four types were

199 comparable across 2020, 2021, and 2022, ranging from 27-30 ppbv for Cluster 1, 38-40 ppbv for Cluster 2, 46-49 ppbv for

200 Cluster 3, and 54-61 ppbv for Cluster 4 (Figure 4c). As depicted in Figure 4d, assuming that the proportions of the four types in

201 2022 are the same as those in 2020 and 2021, the average ozone levels in 2022 would decrease by 14.5% and 17.3%,

202 respectively, remaining comparable to the levels in 2020 and 2021. Alternatively, if the proportions of the four types in 2020 and

203 2021 were the same as those in 2022, the average ozone levels in 2020 and 2021 would increase by 15.4% and 20.2%,

204 respectively, which would be very close to the levels in 2022. Purely statistical analysis indicated that the significant high and

205 stable level of ozone in 2022 was due to a higher proportion of Cluster 3 and Cluster 4, which had higher ozone concentrations

206 during the static management period.
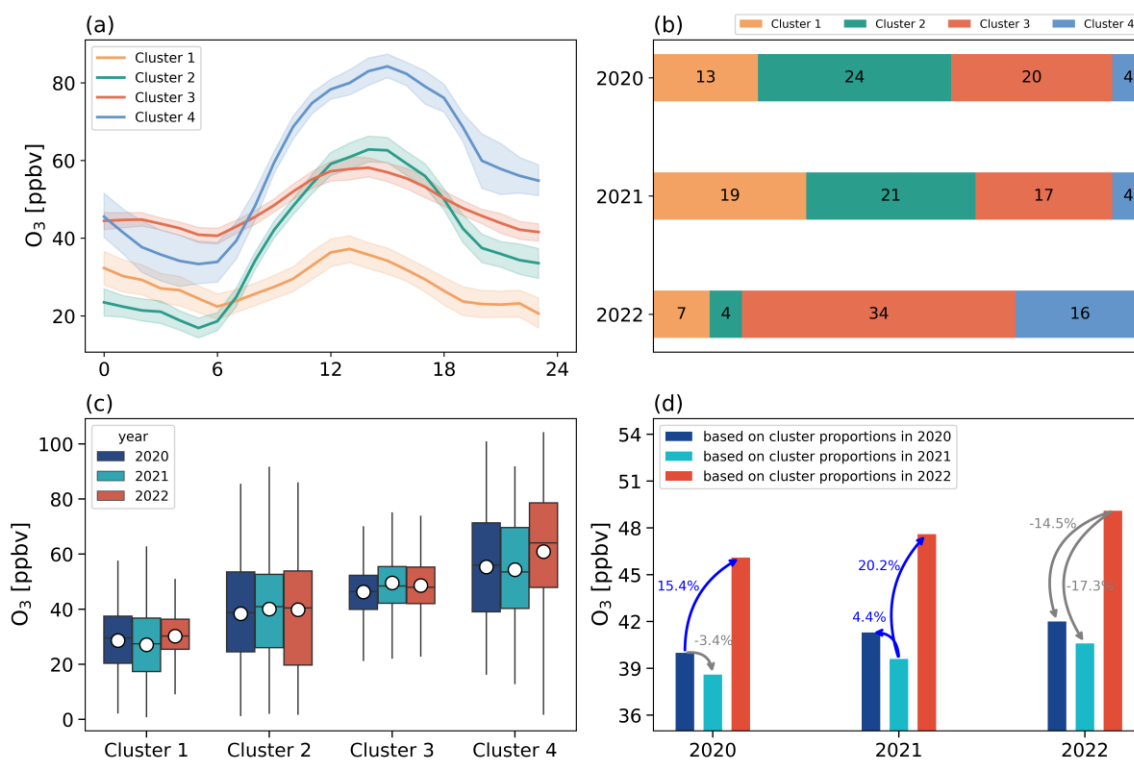
207

208 **Figure 4. (a) Comparison of the mean diurnal profiles of the four types of O₃ after clustering. Colored areas denote 95% confidence**
209 **intervals; (b) The proportions of the four clusters in 2020, 2021 and 2022. (c) Comparison of the O₃ levels of the four clusters in 2020,**
210 **2021 and 2022. The top and bottom of the vertical line for each box correspond to the 95th and 5th percentiles, respectively. The dots**
211 **represent the averages, and the top, middle, and bottom lines of the box mark the 75th, 50th, and 25th percentiles, respectively; (d)**
212 **Comparison of the average ozone concentrations in 2020, 2021 and 2022 for different ratios of the four clusters.**

213 Different types of ozone profiles are formed under different meteorological conditions and pollution environments with

214 distinctive diurnal variations. As shown in Figure 5, the meteorological conditions during the periods of Cluster 2 and Cluster 4,

215 with high net ozone production, were characterized by high temperature, low relative humidity, and high radiation, compared to

216 those during Cluster 1 and Cluster 3 periods. This is consistent with the well-known favorable condition promoting ozone

217 production. The valley values of ozone profiles are closely related to the titration of nitrogen oxides, as shown in Figures 5f and

218 5h, where the valley values of ozone are inversely related to the peak values of NO_2 during the morning rush hour. Indeed, it is

219 these meteorological conditions and titration that result in the formation of the corresponding four clusters of ozone profiles.

220 During periods of Cluster 2 and Cluster 4, a large amount of VOCs accumulated before sunrise and were rapidly consumed after

221 sunrise. Similarly, the precursor NO_2 was also rapidly consumed after sunrise, with the difference that the NO_2 level during

222 Cluster 4 was lower than that of Cluster 2. The diurnal profiles of $PM_{2.5}$ under four clusters exhibit similar patterns to those of

223 VOCs, with Cluster 2 and Cluster 4 exhibiting a distinct morning peak. The VOCs/NO_2 ratio in Cluster 4 was significantly

224 higher than that in other clusters, which may explain the substantial net ozone production despite the relatively high ozone

225 background levels. The differences among the clusters are also reflected in the photochemical processes. In the following

226 sections, we investigated the reasons for the increase in ozone levels during the static management period from the perspective of

227 atmospheric oxidizing capacity and free radical chemistry.
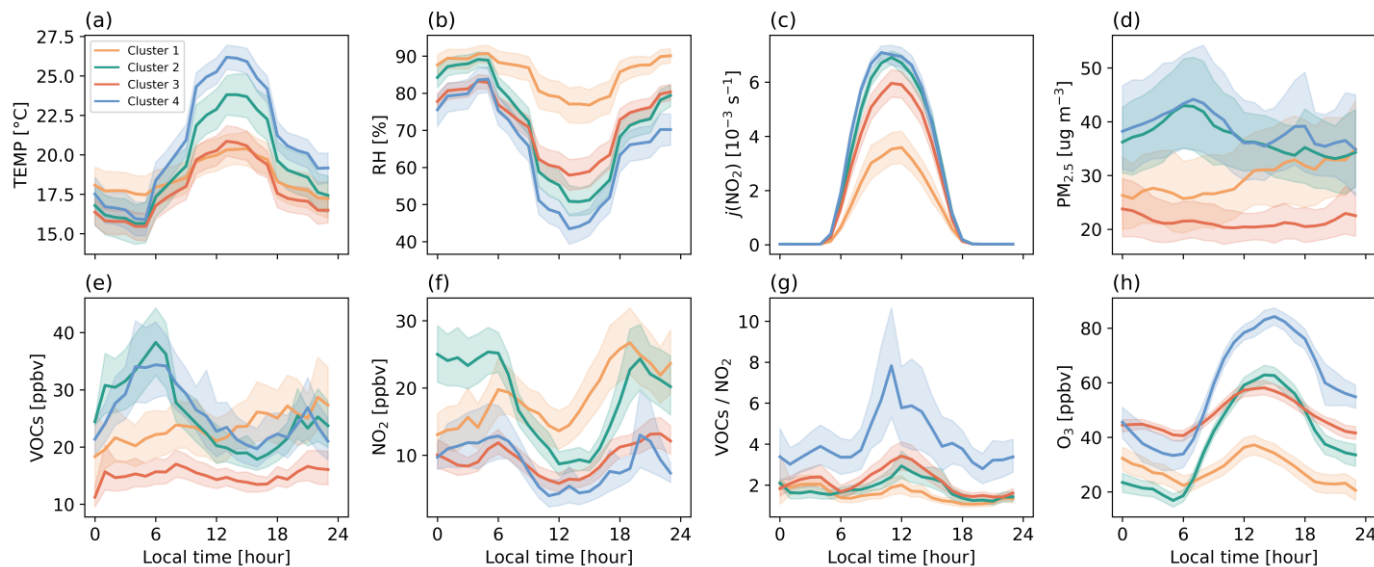
228

229 **Figure 5. The mean diurnal profiles of meteorological parameters and air pollutants for four clusters over three years. Colored areas**
230 **denote 95% confidence intervals.**

231 **3.3 Radical chemistry**

232 Figures 6a, 6e and 6i show the mean diurnal profiles of simulated OH, HO_2 and RO_2 radical concentrations for the years 2020,

233 2021, and 2022. These radicals exhibit clear diurnal variations, with peaks occurring at midday. The mean diurnal profiles

234 display that the average peak concentrations of OH were 5.2×10^6, 4.8×10^6, and 5.1×10^6 molecules cm^{-3}, those of HO_2 were

235 2.2×10^8, 2.7×10^8, and 4.7×10^8 molecules cm^{-3}, and those of RO_2 were 0.9×10^8, 1.6×10^8 and 2.6×10^8 molecules cm^{-3} in

236 2020, 2021 and 2022, respectively. The differences in radicals concentration levels were mainly reflected in the HO_2 and RO_2

237 radicals. The average peak values of the HO_2 and RO_2 radicals in 2022 were about 1 to 3 times higher than those in the same

238 periods of 2020 and 2021. Reviewing previous observational results, peak concentrations of OH and HO_2 were observed at

239 various locations and times (see Table S3): $(4-17) \times 10^6$ molecules cm^{-3} and $(2-24) \times 10^8$ molecules cm^{-3} at a suburban site in

240 Yufa from Aug 18-31, 2006 (Lu et al., 2013); $(5-15) \times 10^6$ molecules cm^{-3} and $(3-14) \times 10^8$ molecules cm^{-3} at a rural site in

241 Wangdu from June 8 to July 8, 2014 (Tan et al., 2017); 4.5×10^6 molecules cm^{-3} and 3×10^8 molecules cm^{-3} at a suburban in

242 Heshan from October 22 to November 5, 2014 (Tan et al., 2019); $(2-9) \times 10^6$ molecules cm^{-3} and $(2-14) \times 10^8$ molecules cm^{-3} at

243 a urban sites in Shenzhen from Oct 5-28, 2018 (Yang et al., 2022); $(8-24) \times 10^6$ molecules cm^{-3} and $(4-28) \times 10^8$ molecules cm^{-3}

244 at a suburban site in Taizhou from May 23 to June 18, 2018 (Ma et al., 2022); and $(10-20) \times 10^6$ molecules cm^{-3} and $(6-18) \times 10^8$

245 molecules cm^{-3} at a suburban site in Chengdu from Aug 10-25, 2019 (Yang et al., 2021). The simulated concentrations of OH

and HO_2 in this study were comparable to the observed levels during autumn in Shenzhen, which is also an urban site, however, were generally lower than those observed at non-urban sites. This difference can be attributed to the site types, but more importantly, to the fact that most observations were conducted during periods of stronger radiation. For RO_2, the average maximum concentration was simulated to be 4.5×10^8 molecules cm^{-3} at urban site of Beijing in August 2007 (Liu et al., 2012). At coastal site of Xiamen, the simulated average daily peak reached 4.7×10^8 molecules cm^{-3} in September 2019, while at the coastal site of Ningde, the simulated value was 0.9×10^8 molecules cm^{-3} in spring 2019 (Liu et al., 2022). Overall, our ROx concentrations fell within the range of observations and simulated results in other regions of China. During the static management period in 2022, the levels of ROx were significantly higher compared to the same period in 2020 and 2021, indicating an enhanced atmospheric oxidation capacity in Shanghai in 2022.

Figures 6b-6d, Figures 6f-6h, and Figures 6j-6l illustrate the mean diurnal variation of primary OH, HO_2, and RO_2 sources for the years of 2020, 2021, and 2022. For OH, HONO photolysis peaked at around 07:00 and remained high until around 12:00, with peak values reaching approximately 0.72 ppbv h^{-1}, 0.52 ppbv h^{-1}, and 0.60 ppbv h^{-1} in 2020, 2021, and 2022, respectively. Meanwhile, ozone photolysis peaked at noon, with peak values reaching around 0.83 ppbv h^{-1}, 0.89 ppbv h^{-1}, and 0.88 ppbv h^{-1}, respectively. In addition, the ozonolysis of unsaturated VOCs was another source of OH radical, with an average production rate of less than 0.10 ppbv h^{-1}, while other sources such as the photolysis of H_2O_2, HNO_3, and OVOCs were generally negligible. Overall, HONO photolysis for the daytime accounted for 57%, 43%, and 48% of the total OH primary production rates in 2020, 2021, and 2022, respectively, with O_3 photolysis accounting for 39%, 48%, and 46% in the corresponding years. For HO_2 radical, the most important source was HCHO photolysis, with average production rates during daytime of 0.28 ppbv h^{-1}, 0.21 ppbv h^{-1}, and 0.25 ppbv h^{-1} in the corresponding years, respectively. The secondary source was OVOCs photolysis, which produce HO_2 at the average rate of 0.14 ppbv h^{-1}, 0.20 ppbv h^{-1}, and 0.08 ppbv h^{-1}, respectively. Another source to consider was reactions of O_3 and unsaturated VOCs, which had an average rate of around 0.07 ppbv h^{-1} for three years. For RO_2 radical, the daytime average peak of primary production rates contributed by OVOCs photolysis from 2020 to 2022 were 0.12 ppbv h^{-1}, 0.16 ppbv h^{-1}, and 0.07 ppbv h^{-1}, respectively. The reactions of O_3 and NO_3 with VOCs were also important primary sources of RO_2 radical. The average daily contributions of O_3+VOC reactions from 2020 to 2022 were 0.09 ppbv h^{-1}, 0.15 ppbv h^{-1}, and 0.08 ppbv h^{-1}, while the contributions of NO_3+VOC reactions were 0.13 ppbv h^{-1}, 0.20 ppbv h^{-1}, and 0.06 ppbv h^{-1}, respectively. The primary production rate of RO_2 in 2022 was lower compared to the years 2020 and 2021. This can be attributed to the fact that the primary sources of RO_2 are the reactions involved VOCs, which significantly decreased during the static management period and further led to the decreased sources of RO_2.

Overall, the total primary production rates of ROx in 2022 was 2.34 ppbv h^{-1}, which is lower than 2.94 ppbv h^{-1} and 2.85 ppbv h^{-1} in 2021, as shown in Figure S13 of the Supplement. . These values are higher than the simulated value of 1.56 ppbv h^{-1} in November 2019 in downtown Shanghai (Zhang et al., 2022a), but close to the value of 2.55 ppbv h^{-1} during the ozone episode in the suburban of Shanghai in 2018 (Zhang et al., 2021). During these three years, reactions involving VOCs (excluding HCHO) accounted for 18.3%, 28.1%, and 26.5%, respectively, which is correlated with the observed VOCs abundances. In 2020 and 2022, HONO photolysis accounted for 30.7% and 28.4% of the total primary production rates, respectively, with O_3 photolysis following at 20.9% and 27.2%. In 2021, the dominant contribution was from O_3 photolysis, reaching 21.4%, followed by HONO photolysis at 19.6%. Radical chemistry exhibits heterogeneity across different cities, with HONO photolysis being a primary source in New York (Ren et al., 2003), Paris (Michoud et al., 2012), Wangdu (Tan et al., 2017), and Taizhou (Ma et al., 2022). OVOC photolysis dominated in Mexico City (Sheehy et al., 2010), Hong Kong (Xue et al., 2016), and Beijing (Liu et al., 2012). Milan relied on HCHO photolysis as a major source (Alicke et al., 2002), while ozone photolysis was prominent in Nashville (Martinez et al., 2003).
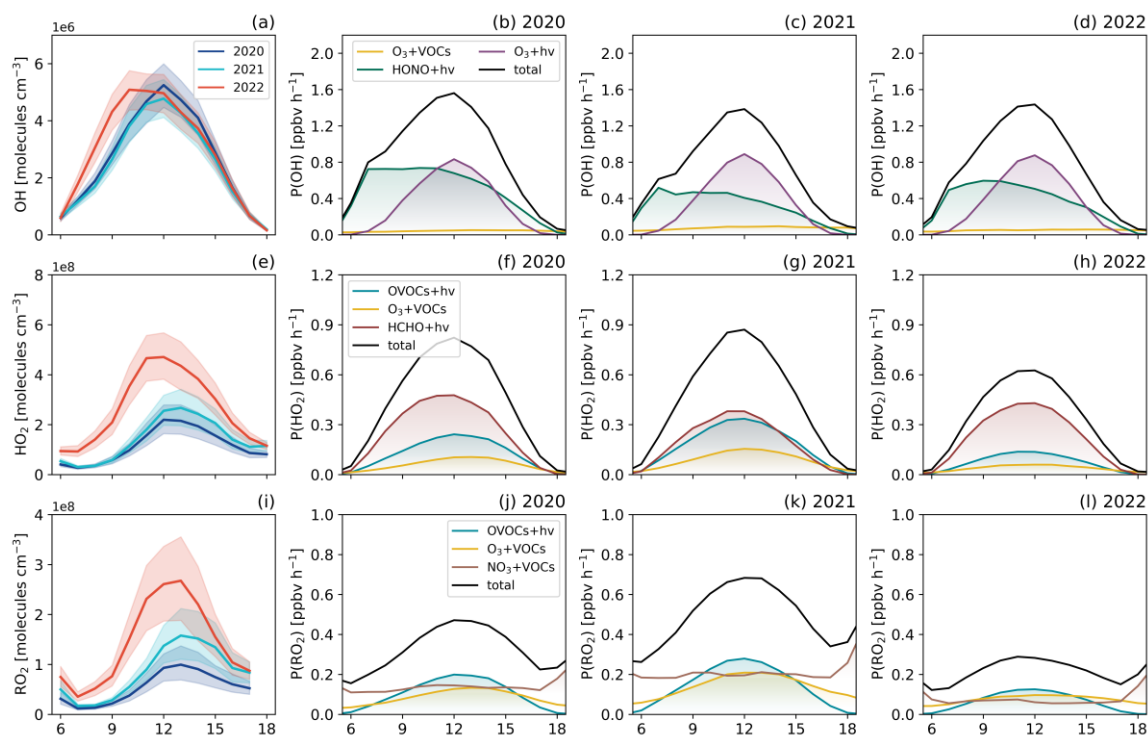
Figure 6. The mean diurnal profiles of simulated OH (a), HO₂ (e), and RO₂ (i) concentrations in 2020, 2021, and 2022. Colored areas denote 95% confidence intervals; The mean diurnal profiles of primary sources of OH radical (b-d), HO₂ radical (f-h), and RO₂ radical (j-l) from model calculations in 2020, 2021 and 2022.

We also investigated the radical chemistry under different ozone profile clusters (Figure 7). The average peak of OH in Cluster 1, Cluster 2, Cluster 3, and Cluster 4 were 2.6×10^6 molecules cm^{-3}, 5.9×10^6 molecules cm^{-3}, 5.4×10^6 molecules cm^{-3}, and 6.4×10^6 molecules cm^{-3}, those of HO₂ were 1.1×10^8 molecules cm^{-3}, 2.9×10^8 molecules cm^{-3}, 3.3×10^8 molecules cm^{-3}, and 6.1×10^8 molecules cm^{-3}, and those of RO₂ were 0.5×10^8 molecules cm^{-3}, 1.7×10^8 molecules cm^{-3}, 1.5×10^8 molecules cm^{-3}, and 4.5×10^8 molecules cm^{-3}, respectively. Clearly, Cluster 4 had the highest levels of OH, HO₂, and RO₂ radicals among all clusters, with HO₂ and RO₂ radicals being particularly prominent. The average peak of P(ROx) for Clusters 1 to 4 were 1.71 ppbv h-1, 3.58 ppbv h-1, 2.39 ppbv h-1, and 3.77 ppbv h-1, respectively. Cluster 2 and Cluster 4, characterized by significant net ozone production, exhibit distinct features in radical chemistry. The daily average of P(ROx) was 2.28 ppbv h^{-1} in Cluster 2 and 2.37 ppbv h^{-1} in Cluster 4, which is higher than the values of 1.08 ppbv h^{-1} in Cluster 1 and 1.44 ppbv h^{-1} in Cluster 3. In addition, HONO photolysis during the morning rush hour was particularly prominent in Cluster 2 and Cluster 4, with peak values reaching 0.99 ppbv h^{-1} and 0.83 ppbv h^{-1}, respectively. In Cluster 2, HONO photolysis was the dominant source with a daily average of 0.56 ppbv h^{-1}, accounting for 25% of the total, and ozone photolysis followed with 0.47 ppbv h^{-1}, accounting for 21%. On the other hand, in Cluster 4, ozone photolysis took the lead with 0.65 ppbv h^{-1}, representing 27% of the total, and HONO photolysis came next with 0.47 ppbv h^{-1}, accounting for 20%. Additionally, OVOCs photolysis (including HCHO) in Cluster 2 and Cluster 4 showed a significant increase compared to Cluster 1 and Cluster 3. The correlation analysis between the each primary source of radicals and the net ozone production reveals a significant correlation (see Figure S15), which shows that a large amount of net ozone production implies the presence of active photochemical processes. Cluster 4 is characterized by higher concentrations of HO₂ and RO₂ radicals and a higher primary source of radicals. Cluster 3 has moderate levels of radical concentrations and primary sources of radicals, but it features a high ozone background value. The increase in the number of days associated with these two clusters in 2022 has contributed to the elevated ozone levels.
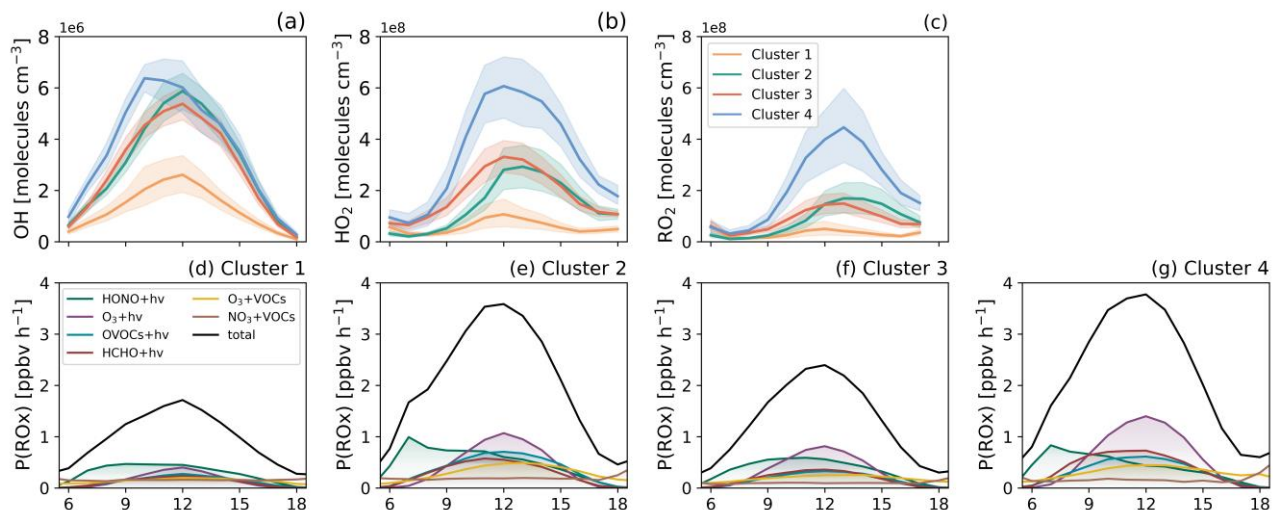
Figure 7. The mean diurnal profiles of simulated OH (a), HO$_2$ (b), and RO$_2$ (c) concentrations for Cluster 1, Cluster 2, Cluster 3, and Cluster 4. Colored areas denote 95% confidence intervals; The mean diurnal profiles of primary sources of ROx radical (d-g) from model calculations for Cluster 1, Cluster 2, Cluster 3, and Cluster 4.

In tropospheric chemistry, radical initiation, which involves the breakdown of closed-shell species to generate new radicals, plays a crucial role in initiating the formation of secondary pollutants. However, in highly polluted atmospheric environments, radical cycling becomes the dominant process, with the amplification of new radicals in the ROx cycle playing a crucial role. Volkamer et al. (2010) quantified the production of new radicals and found that approximately 20% of radical production is attributed to the breakdown of closed-shell species, while 80% is derived from radical cycling. Therefore, in addition to understanding the sources of radicals, it is essential to comprehend the impacts of radical cycling and recycling processes on ozone formation. Figure 8 demonstrated the daytime average of ROx radicals budgets during the periods from April to May of 2020, 2021, and 2022. Taking the simulation of 2022 as an example, OH oxidation of CO and VOCs produces HO$_2$ and RO$_2$ with daytime average rates of 2.09 ppbv h^{-1} (1.90 ppbv h^{-1} in 2020 and 1.77 ppbv h^{-1} in 2021) and 1.20 ppbv h^{-1} (1.20 ppbv h^{-1} in 2020 and 1.55 ppbv h^{-1} in 2021), respectively. The reactions of RO$_2$+NO and HO$_2$+NO further lead to the strong production of RO with a rate of 1.50 ppbv h^{-1} (1.85 ppbv h^{-1} in 2020 and 2.51 ppbv h^{-1} in 2021) and OH with a rate of 3.44 ppbv h^{-1} (3.91 ppbv h^{-1} in 2020 and 4.07 ppbv h^{-1} in 2021), while generating O$_3$ as a by-product. Clearly, these recycling processes dominate the overall production of ROx radicals compared to the primary sources. The OH-HO$_2$ cycle is an important process in ozone formation. According to the statistics in Table S3, no evidence was found to suggest that the cycle in 2022 was more efficient than in 2020 and 2021. In terms of termination processes, the loss of ROx radicals was primarily dominated by their reactions with NOx. Specifically, the reactions of OH+NO$_2$ and RO$_2$+NO$_2$ accounted for approximately 0.51 ppbv h^{-1} (1.01 ppbv h^{-1} in 2020 and 0.87 ppbv h^{-1} in 2021) and 0.21 ppbv h^{-1} (0.25 ppbv h^{-1} in 2020 and 0.30 ppbv h^{-1} in 2021) of the ROx radical loss on daytime average, respectively. This is in line with the understanding that reactions involving NOx typically play a dominant role in the removal of radicals in high NOx environments (Zhang et al., 2021; Xue et al., 2016; Volkamer et al., 2010; Tan et al., 2019; Liu et al., 2012). To sum up, the changes resulting from the approximately 55% reduction in NO$_2$ and 30% reduction in VOCs due to static management are reflected in both the radical propagation and termination processes. The ratio of OH radical propagation (OH+VOCs) to termination (OH+NO$_2$) reached 2.37, which is higher than 1.18 in 2020 and 1.78 in 2021. It can be inferred the different proportions of NO$_2$ and VOCs reduction did not weaken the radical cycling. On the contrary, a higher VOCs/NO$_2$ ratio promotes the radical recycling efficiency in the reaction chain of radicals.
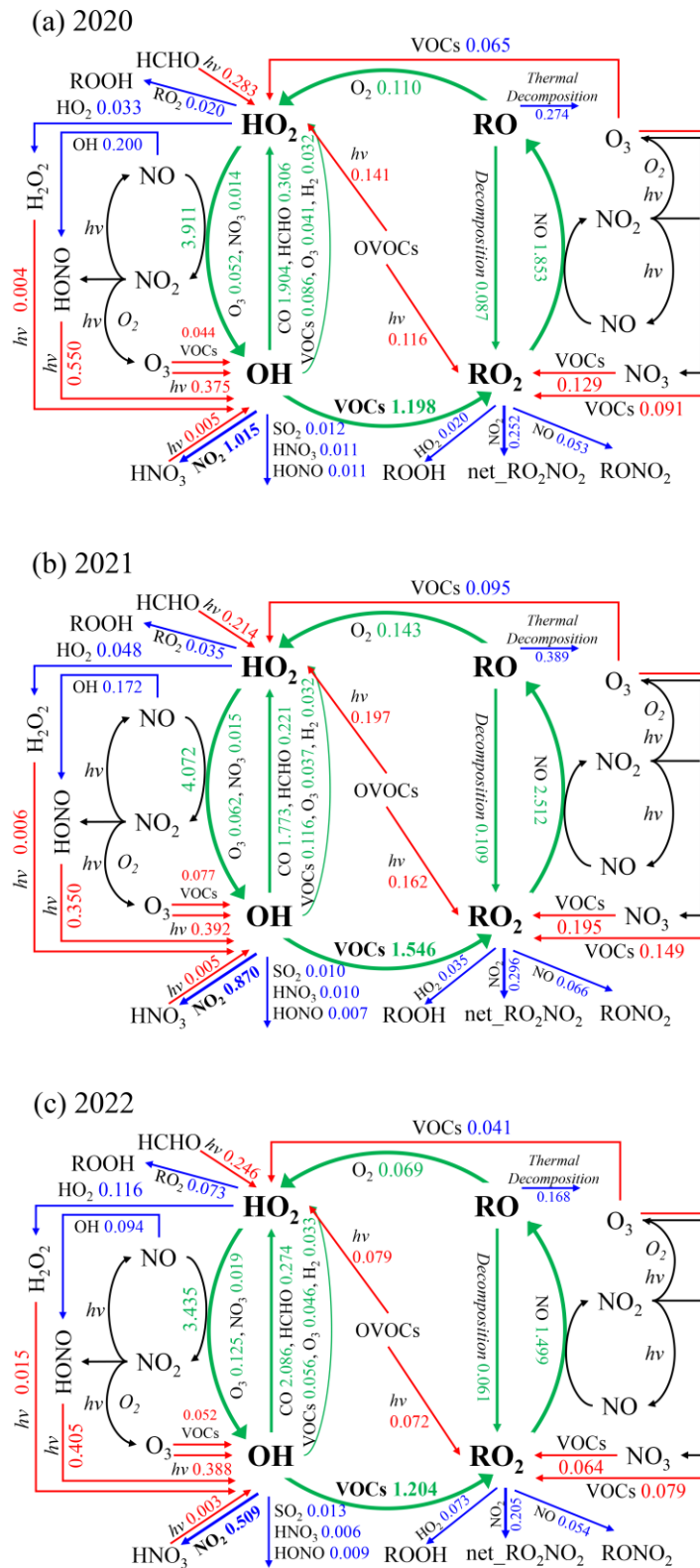
Figure 8. Averaged budgets (in ppbv h⁻¹) of ROx radicals in daytime (06:00-18:00) during the periods from April to May of 2020, 2021, and 2022. The red, blue, and green lines and words indicate the primary production, termination, and recycling pathways of radicals, respectively.

4 Conclusions

The two-month city-wide static management was implemented in April and May 2022 in Shanghai aiming to control the spread of the Omicron variant, providing a valuable opportunity to study the causes of ozone pollution. The comprehensive observations during the static management and same period in 2020 and 2021 show that there was a decrease of 29%-35% in VOCs and 51%-55% in NO_2 concentrations, while the average ozone level increased by nearly 23%. By statistics, the ozone profiles were classified into four clusters: Cluster 1, characterized by low background concentration and low net production; Cluster 2, characterized by low background concentration and high net production; Cluster 3, characterized by high background concentration and low net production; and Cluster 4, characterized by high background concentration and high net production. The average O_3 concentration relationship among these clusters is Cluster 4 > Cluster 3 > Cluster 2 > Cluster 1. The significant increase in the proportion of Cluster 4 and Cluster 3 during the period of static management led to an overall increase in average ozone levels. Secondly, from the perspective of radical chemistry, we explored the changes in photochemical processes due to the reduction in precursor species. The OBM model simulated the levels of radicals and their processes of initiation, propagation, and termination. The average peak concentrations of OH, HO_2, and RO_2 in 2022 were 5.1×10^6, 4.7×10^8, and 2.6×10^8 molecules cm^{-3}, respectively, which were higher than those in the same period in 2020 and 2021. HONO photolysis was the main contributor to the primary source of ROx, accounting for about 30% of the total. However, in terms of the overall production of ROx radicals, the radical recycling process remained dominant. The different proportions of NO_2 and VOCs redution during static management led to an increased OH radical propagation (OH+VOCs) to termination (OH+NO_2) ratio, reaching 2.37, higher than 1.18 in 2020 and 1.78 in 2021. This enhanced ratio indicates a strengthened radical cycling as a result of a higher VOCs/NO_2 ratio.

The important lesson from the static management "large-scale field experiment" is that Shanghai operates in a VOCs-limited regime. When the reduction in VOCs is not able to catch up with or exceed the reduction in nitrogen oxides, it is not sufficient to curb the formation of secondary pollutants. In terms of ozone control strategies, it is necessary to strengthen the regulation and control of VOCs.

Data Availability

The observed and predicted hourly time series data in the study are presented in Figure S16-S18, and Code and data used for our analyses are available at *https://data.mendeley.com/datasets/3kmhg7r2df/1*(Zhu, 2023).

Competing interests

The contact author has declared that none of the authors has any competing interests.

Author contributions

Jian Zhu: Conceptualization, Methodology, Software, Validation, Investigation, Writing original draft, Visualization. Shanshan Wang: Conceptualization, Methodology, Supervision, Funding acquisition. Chuanqi Gu, Zhiwen Jiang, Sanbao Zhang, Ruibin Xue, and Yuhao Yan: Methodology, Validation, Investigation. Bin Zhou: Conceptualization, Methodology, Supervision, Funding acquisition.

Acknowledgments

This work was supported by National Natural Science Foundation of China (22176037, 42075097, 22376030, 42375089, 21976031) and National Key Research and Development Program of China(2022YFC3700101).

References

Agarwal, A., Kaushik, A., Kumar, S., and Mishra, R. K.: Comparative study on air quality status in Indian and Chinese cities before and during the COVID-19 lockdown period, Air Quality, Atmosphere & Health, 13, 1167-1178, https://doi.org/10.1007/s11869-020-00881-z, 2020.

Alicke, B., Platt, U., and Stutz, J.: Impact of nitrous acid photolysis on the total hydroxyl radical budget during the Limitation of Oxidant Production/Pianura Padana Produzione di Ozono study in Milan, Journal of Geophysical Research: Atmospheres, 107, LOP 9-1-LOP 9-17, https://doi.org/10.1029/2000JD000075, 2002.

Bao, R. and Zhang, A.: Does lockdown reduce air pollution? Evidence from 44 cities in northern China, Science of the Total Environment, 731, 139052, https://doi.org/10.1016/j.scitotenv.2020.139052, 2020.

Cai, C., Geng, F., Tie, X., Yu, Q., and An, J.: Characteristics and source apportionment of VOCs measured in Shanghai, China, Atmospheric Environment, 44, 5005-5014, https://doi.org/10.1016/j.atmosenv.2010.07.059, 2010.

Chu, B., Zhang, S., Liu, J., Ma, Q., and He, H.: Significant concurrent decrease in $PM_{2.5}$ and NO_2 concentrations in China during COVID-19 epidemic, Journal of Environmental Sciences, 99, 346-353, https://doi.org/10.1016/j.jes.2020.06.031, 2021.

Darby, L. S.: Cluster analysis of surface winds in Houston, Texas, and the impact of wind patterns on ozone, Journal of Applied Meteorology and Climatology, 44, 1788-1806, https://doi.org/10.1175/JAM2320.1, 2005.

Ding, J., van der A, R. J., Eskes, H., Mijling, B., Stavrakou, T., Van Geffen, J., and Veefkind, J.: NOx emissions reduction and rebound in China due to the COVID-19 crisis, Geophysical Research Letters, 47, e2020GL089912, https://doi.org/10.1029/2020GL089912, 2020.

Feng, S., Jiang, F., Wang, H., Wang, H., Ju, W., Shen, Y., Zheng, Y., Wu, Z., and Ding, A.: NOx emission changes over China during the COVID-19 epidemic inferred from surface NO2 observations, Geophysical Research Letters, 47, e2020GL090080, https://doi.org/10.1029/2020GL090080, 2020.

Gu, C., Wang, S., Zhu, J., Wu, S., Duan, Y., Gao, S., and Zhou, B.: Investigation on the urban ambient isoprene and its oxidation processes, Atmospheric Environment, 270, 118870, https://doi.org/10.1016/j.atmosenv.2021.118870, 2022.

Guo, Y., Wang, S., Zhu, J., Zhang, R., Gao, S., Saiz-Lopez, A., and Zhou, B.: Atmospheric formaldehyde, glyoxal and their relations to ozone pollution under low-and high-NOx regimes in summertime Shanghai, China, Atmospheric Research, 258, 105635, https://doi.org/10.1016/j.atmosres.2021.105635, 2021.

Hua, J., Zhang, Y., de Foy, B., Shang, J., Schauer, J. J., Mei, X., Sulaymon, I. D., and Han, T.: Quantitative estimation of meteorological impacts and the COVID-19 lockdown reductions on NO_2 and $PM_{2.5}$ over the Beijing area using Generalized Additive Models (GAM), Journal of Environmental Management, 291, 112676, https://doi.org/10.1016/j.jenvman.2021.112676, 2021.

Huang, X., Ding, A., Gao, J., Zheng, B., Zhou, D., Qi, X., Tang, R., Wang, J., Ren, C., and Nie, W.: Enhanced secondary pollution offset reduction of primary emissions during COVID-19 lockdown in China, National Science Review, 8, nwaa137, https://doi.org/10.1093/nsr/nwaa137, 2021.

Jenkin, M., Saunders, S., Wagner, V., and Pilling, M.: Protocol for the development of the Master Chemical Mechanism, MCM v3 (Part B): tropospheric degradation of aromatic volatile organic compounds, Atmospheric Chemistry and Physics, 3, 181-193, https://doi.org/10.5194/acp-3-181-2003, 2003.

Li, D., Wang, S., Xue, R., Zhu, J., Zhang, S., Sun, Z., and Zhou, B.: OMI-observed HCHO in Shanghai, China, during 2010–2019 and ozone sensitivity inferred by an improved $HCHO/NO_2$ ratio, Atmospheric Chemistry and Physics, 21, 15447-15460, https://doi.org/10.5194/acp-21-15447-2021, 2021a.

Li, R., Zhao, Y., Fu, H., Chen, J., Peng, M., and Wang, C.: Substantial changes in gaseous pollutants and chemical compositions in fine particles in the North China Plain during the COVID-19 lockdown period: anthropogenic vs. meteorological influences, Atmospheric Chemistry and Physics, 21, 8677-8692, https://doi.org/10.5194/acp-21-8677-2021, 2021b.

Liu, C. and Shi, K.: A review on methodology in O_3-NOx-VOC sensitivity study, Environmental Pollution, 291, 118249, https://doi.org/10.1016/j.envpol.2021.118249, 2021.

Liu, T., Hong, Y., Li, M., Xu, L., Chen, J., Bian, Y., Yang, C., Dan, Y., Zhang, Y., and Xue, L.: Atmospheric oxidation capacity and ozone pollution mechanism in a coastal city of southeastern China: analysis of a typical photochemical episode by an observation-based model, Atmospheric Chemistry and Physics, 22, 2173-2190, https://doi.org/10.5194/acp-22-2173-2022, 2022.

Liu, T., Wang, X., Hu, J., Wang, Q., An, J., Gong, K., Sun, J., Li, L., Qin, M., and Li, J.: Driving forces of changes in air quality during the COVID-19 lockdown period in the Yangtze River Delta Region, China, Environmental Science & Technology Letters, 7, 779-786, https://doi.org/10.1021/acs.estlett.0c00511, 2020.

Liu, Y., Wang, H., Jing, S., Gao, Y., Peng, Y., Lou, S., Cheng, T., Tao, S., Li, L., and Li, Y.: Characteristics and sources of volatile organic compounds (VOCs) in Shanghai during summer: Implications of regional transport, Atmospheric Environment, 215, 116902, https://doi.org/10.1016/j.atmosenv.2019.116902, 2019.

Liu, Z., Wang, Y., Gu, D., Zhao, C., Huey, L. G., Stickel, R., Liao, J., Shao, M., Zhu, T., and Zeng, L.: Summertime photochemistry during CAREBeijing-2007: ROx budgets and O_3 formation, Atmospheric Chemistry and Physics, 12, 7737-7752, https://doi.org/10.5194/acp-12-7737-2012, 2012.

Lu, K., Hofzumahaus, A., Holland, F., Bohn, B., Brauers, T., Fuchs, H., Hu, M., Häseler, R., Kita, K., and Kondo, Y.: Missing OH source in a suburban environment near Beijing: observed and modelled OH and HO_2 concentrations in summer 2006, Atmospheric Chemistry and Physics, 13, 1057-1080, https://doi.org/10.5194/acp-13-1057-2013, 2013.

Ma, X., Tan, Z., Lu, K., Yang, X., Chen, X., Wang, H., Chen, S., Fang, X., Li, S., and Li, X.: OH and HO_2 radical chemistry at a suburban site during the EXPLORE-YRD campaign in 2018, Atmospheric Chemistry and Physics, 22, 7005-7028, https://doi.org/10.5194/acp-22-7005-2022, 2022.

Martinez, M., Harder, H., Kovacs, T., Simpas, J., Bassis, J., Lesher, R., Brune, W., Frost, G., Williams, E., and Stroud, C.: OH and HO_2 concentrations, sources, and loss rates during the Southern Oxidants Study in Nashville, Tennessee, summer 1999, Journal of Geophysical Research: Atmospheres, 108, https://doi.org/10.1029/2003JD003551, 2003.

Michoud, V., Kukui, A., Camredon, M., Colomb, A., Borbon, A., Miet, K., Aumont, B., Beekmann, M., Durand-Jolibois, R., and Perrier, S.: Radical budget analysis in a suburban European site during the MEGAPOLI summer field campaign, Atmospheric Chemistry and Physics, 12, 11951-11974, https://doi.org/10.5194/acp-12-11951-2012, 2012.

Rana, R. H., Keramat, S. A., and Gow, J.: A systematic literature review of the impact of COVID-19 lockdowns on air quality in China, Aerosol and Air Quality Research, 21, 200614, https://doi.org/10.4209/aaqr.200614, 2021.

Ren, X., Harder, H., Martinez, M., Lesher, R. L., Oliger, A., Shirley, T., Adams, J., Simpas, J. B., and Brune, W. H.: HOx concentrations and OH reactivity observations in New York City during PMTACS-NY2001, Atmospheric Environment, 37, 3627-3637, https://doi.org/10.1016/S1352-2310(03)00460-6, 2003.

Santiago, J.-L., Martilli, A., and Martin, F.: On dry deposition modelling of atmospheric pollutants on vegetation at the microscale: Application to the impact of street vegetation on air quality, Boundary-layer meteorology, 162, 451-474, https://doi.org/10.1007/s10546-016-0210-5, 2017.

Saunders, S. M., Jenkin, M. E., Derwent, R., and Pilling, M.: Protocol for the development of the Master Chemical Mechanism, MCM v3 (Part A): tropospheric degradation of non-aromatic volatile organic compounds, Atmospheric Chemistry and Physics, 3, 161-180, https://doi.org/10.5194/acp-3-161-2003, 2003.

Sheehy, P., Volkamer, R., Molina, L. T., and Molina, M. J.: Oxidative capacity of the Mexico City atmosphere-Part 2: A ROx radical cycling perspective, Atmospheric Chemistry and Physics, 10, 6993-7008, https://doi.org/10.5194/acp-10-6993-2010, 2010.

Shi, X. and Brasseur, G. P.: The response in air quality to the reduction of Chinese economic activities during the COVID-19 outbreak, Geophysical Research Letters, 47, e2020GL088070, https://doi.org/10.1029/2020GL088070, 2020.

Sillman, S.: The relation between ozone, NOx and hydrocarbons in urban and polluted rural environments, Atmospheric Environment, 33, 1821-1845, https://doi.org/10.1016/S1352-2310(98)00345-8, 1999.

Sommariva, R., Cox, S., Martin, C., Borońska, K., Young, J., Jimack, P. K., Pilling, M. J., Matthaios, V. N., Nelson, B. S., and Newland, M. J.: AtChem (version 1), an open-source box model for the Master Chemical Mechanism, Geoscientific Model Development, 13, 169-183, https://doi.org/10.5194/gmd-13-169-2020, 2020.

Suris, F. N. A., Bakar, M. A. A., Ariff, N. M., Mohd Nadzir, M. S., and Ibrahim, K.: Malaysia PM_{10} air quality time series clustering based on dynamic time warping, Atmosphere, 13, 503, https://doi.org/10.3390/atmos13040503, 2022.

Tan, Y. and Wang, T.: What caused ozone pollution during the 2022 Shanghai lockdown? Insights from ground and satellite observations, Atmospheric Chemistry and Physics, 22, 14455-14466, https://doi.org/10.5194/acp-22-14455-2022, 2022.

Tan, Z., Fuchs, H., Lu, K., Hofzumahaus, A., Bohn, B., Broch, S., Dong, H., Gomm, S., Häseler, R., and He, L.: Radical chemistry at a rural site (Wangdu) in the North China Plain: observation and model calculations of OH, HO_2 and RO_2 radicals, Atmospheric Chemistry and Physics, 17, 663-690, https://doi.org/10.5194/acp-17-663-2017, 2017.

Tan, Z., Lu, K., Hofzumahaus, A., Fuchs, H., Bohn, B., Holland, F., Liu, Y., Rohrer, F., Shao, M., and Sun, K.: Experimental budgets of OH, HO_2, and RO_2 radicals and implications for ozone formation in the Pearl River Delta in China 2014, Atmospheric chemistry and physics, 19, 7129-7150, https://doi.org/10.5194/acp-19-7129-2019, 2019.

Tian, J., Wang, Q., Zhang, Y., Yan, M., Liu, H., Zhang, N., Ran, W., and Cao, J.: Impacts of primary emissions and secondary aerosol formation on air pollution in an urban area of China during the COVID-19 lockdown, Environment International, 150, 106426, https://doi.org/10.1016/j.envint.2021.106426, 2021.

Venter, Z. S., Aunan, K., Chowdhury, S., and Lelieveld, J.: COVID-19 lockdowns cause global air pollution declines, Proceedings of the National Academy of Sciences, 117, 18984-18990, https://doi.org/10.1073/pnas.200685311, 2020.

Volkamer, R., Sheehy, P., Molina, L. T., and Molina, M. J.: Oxidative capacity of the Mexico City atmosphere-Part 1: A radical source perspective, Atmospheric Chemistry and Physics, 10, 6969-6991, https://doi.org/10.5194/acp-10-6969-2010, 2010.

Wang, N., Xu, J., Pei, C., Tang, R., Zhou, D., Chen, Y., Li, M., Deng, X., Deng, T., and Huang, X.: Air quality during COVID-19 lockdown in the Yangtze River Delta and the Pearl River Delta: Two different responsive mechanisms to emission reductions in China, Environmental Science & Technology, 55, 5721-5730, https://doi.org/10.1021/acs.est.0c08383, 2021.

Wang, P., Chen, K., Zhu, S., Wang, P., and Zhang, H.: Severe air pollution events not avoided by reduced anthropogenic activities during COVID-19 outbreak, Resources, Conservation and Recycling, 158, 104814, https://doi.org/10.1016/j.resconrec.2020.104814, 2020.

Wang, T., Xue, L., Brimblecombe, P., Lam, Y. F., Li, L., and Zhang, L.: Ozone pollution in China: A review of concentrations, meteorological influences, chemical precursors, and effects, Science of the Total Environment, 575, 1582-1596, https://doi.org/10.1016/j.scitotenv.2016.10.081, 2017.

Xue, L., Gu, R., Wang, T., Wang, X., Saunders, S., Blake, D., Louie, P. K., Luk, C. W., Simpson, I., and Xu, Z.: Oxidative capacity and radical chemistry in the polluted atmosphere of Hong Kong and Pearl River Delta region: analysis of a severe photochemical smog episode, Atmospheric Chemistry and Physics, 16, 9891-9903, https://doi.org/10.5194/acp-16-9891-2016, 2016.

Xue, R., Wang, S., Zhang, S., Zhan, J., Zhu, J., Gu, C., and Zhou, B.: Ozone Pollution of Megacity Shanghai during City‑Wide Lockdown Assessed Using TROPOMI Observations of NO_2 and HCHO, Remote Sensing, 14, 6344, https://doi.org/10.3390/rs14246344, 2022.

Yang, X., Lu, K., Ma, X., Gao, Y., Tan, Z., Wang, H., Chen, X., Li, X., Huang, X., and He, L.: Radical chemistry in the Pearl River Delta: observations and modeling of OH and HO_2 radicals in Shenzhen in 2018, Atmospheric Chemistry and Physics, 22, 12525-12542, https://doi.org/10.5194/acp-22-12525-2022, 2022.

Yang, X., Lu, K., Ma, X., Liu, Y., Wang, H., Hu, R., Li, X., Lou, S., Chen, S., and Dong, H.: Observations and modeling of OH and HO_2 radicals in Chengdu, China in summer 2019, Science of The Total Environment, 772, 144829, https://doi.org/10.1016/j.scitotenv.2020.144829, 2021.

Zhang, G., Hu, R., Xie, P., Lou, S., Wang, F., Wang, Y., Qin, M., Li, X., Liu, X., and Wang, Y.: Observation and simulation of HOx radicals in an urban area in Shanghai, China, Science of The Total Environment, 810, 152275, https://doi.org/10.1016/j.scitotenv.2021.152275, 2022a.

Zhang, K., Huang, L., Li, Q., Huo, J., Duan, Y., Wang, Y., Yaluk, E., Wang, Y., Fu, Q., and Li, L.: Explicit modeling of isoprene chemical processing in polluted air masses in suburban areas of the Yangtze River Delta region: radical cycling and formation of ozone and formaldehyde, Atmospheric Chemistry and Physics, 21, 5905-5917, https://doi.org/10.5194/acp-21-5905-2021, 2021.

Zhang, K., Liu, Z., Zhang, X., Li, Q., Jensen, A., Tan, W., Huang, L., Wang, Y., de Gouw, J., and Li, L.: Insights into the significant increase in ozone during COVID-19 in a typical urban city of China, Atmospheric Chemistry and Physics, 22, 4853-4866, https://doi.org/10.5194/acp-22-4853-2022, 2022b.

Zhu, J.: Why Did Ozone Concentrations Increase During Shanghai's Static Management? A Statistical and Radical Chemistry Perspective (V1), Mendeley Data [dataset], 10.17632/3kmhg7r2df.1, 2023.

Zhu, J., Wang, S., Zhang, S., Xue, R., Gu, C., and Zhou, B.: Changes of NO_3 Radical and its Nocturnal Chemistry in Shanghai from 2014 to 2021 Revealed by Long-term observation and a Stacking Model: Impact of China's Clean Air Action Plan, Journal of Geophysical Research: Atmospheres, e2022JD037438, https://doi.org/10.1029/2022JD037438, 2022.

Zhu, J., Wang, S., Wang, H., Jing, S., Lou, S., Saiz-Lopez, A., and Zhou, B.: Observationally constrained modeling of atmospheric oxidation capacity and photochemical reactivity in Shanghai, China, Atmospheric Chemistry and Physics, 20, 1217-1232, https://doi.org/10.5194/acp-20-1217-2020, 2020.